Received: 15 June 2018 | Revised: 1 October 2018 | Accepted: 15 October 2018

DOI: 10.1002/pip.3088

EU PVSEC PAPER

WILEY PROGRESS IN PHOTOVOLTAICS

Impact of black silicon on light- and elevated temperature-induced degradation in industrial passivated emitter and rear cells

Toni P. Pasanen[1] | Chiara Modanese[1] | Ville Vähänissi[1] | Hannu S. Laine[1] | Franziska Wolny[2] | Alexander Oehlke[2] | Christian Kusterer[2] | Ismo T.S. Heikkinen[1,3] | Matthias Wagner[2] | Hele Savin[1]

[1] Department of Electronics and Nanoengineering, Aalto University, Tietotie 3, 02150 Espoo, Finland

[2] SolarWorld Industries GmbH, Martin-Luther-King-Str. 24, 53175 Bonn, Germany

[3] Beneq Oy, Olarinluoma 9, 02200 Espoo, Finland

Correspondence
Toni Pasanen, Department of Electronics and Nanoengineering, Aalto University, Tietotie 3, 02150 Espoo, Finland.
Email: toni.pasanen@aalto.fi

Funding information
FP7 Ideas: European Research Council, Grant/Award Number: 307315; Tekes, Grant/Award Number: 2956/31/2014; Tiina & Antti Herlin Foundation; Finnish Cultural Foundation; Walter Ahlström Foundation; Jenny and Antti Wihuri Foundation; Aalto ELEC Doctoral School; SOLAR-ERA.NET

Abstract

Light and elevated-temperature induced degradation (LeTID) is currently a severe issue in passivated emitter and rear cells (PERC). In this work, we study the impact of surface texture, especially a black silicon (b-Si) nanostructure, on LeTID in industrial p-type mc-Si PERC. Our results show that during standard LeTID conditions the b-Si cells with atomic-layer-deposited aluminum oxide (AlO_x) front surface passivation show no degradation despite the presence of a hydrogen-rich AlO_x/SiN_x passivation stack on the rear. Furthermore, b-Si solar cells passivated with silicon nitride (SiN_x) on the front lose only 1.5%$_{rel}$ of their initial power conversion efficiency, while the acidic-textured equivalents degrade by nearly 4%$_{rel}$ under the same conditions. Correspondingly, clear degradation is visible in the internal quantum efficiency (IQE) of the acidic-textured cells, especially in the ~850 to 1100-nm wavelength range confirming that the degradation occurs in the bulk, while the IQE remains nearly unaffected in the b-Si cells. The observations are supported by spatially resolved photoluminescence (PL) maps, which show a clear contrast in the degradation behavior of b-Si and acidic-textured cells, especially in the case of SiN_x front surface passivation. The PL maps also suggest that the magnitude of LeTID scales with surface area of the texture, rather than wafer thickness that was recently reported, although the b-Si cells are slightly thinner (140 vs 165 μm). The results indicate that b-Si has a positive impact on LeTID, and hence, benefits provided by b-Si are not limited only to the excellent optical properties, as commonly understood.

KEYWORDS

black silicon, light- and elevated temperature-induced degradation, light-induced degradation, multicrystalline silicon, passivated emitter and rear cells, solar cells

1 | INTRODUCTION

The capability to eliminate reflective losses of diamond wire-sawn multicrystalline silicon (mc-Si) wafers has made black silicon (nanostructured silicon, b-Si) of particular interest within the photovoltaics (PV) community.[1,2] Furthermore, the large surface area of b-Si is no longer a hindrance for high-efficiency b-Si solar cells due to the advancements in novel surface passivation methods.[1,3-5] In fact, it has been recently shown that the large surface area can provide also an advantage, since it significantly enhances gettering of deleterious metal impurities during phosphorus diffusion.[6]

The evidence for enhanced gettering implies that b-Si could also influence light- and elevated temperature-induced degradation (LeTID), which is the main culprit for efficiency deterioration in today's

multicrystalline silicon (mc-Si) solar cells.[7,8] LeTID may result in over 10% relative efficiency loss in cells with dielectrically-passivated rear side,[7,9,10] which is a significant issue for the PV industry that is shifting towards passivated emitter and rear cells (PERC).[2] Hence, several PV research groups, academic institutions, and companies have recently investigated methods to mitigate the detrimental phenomenon, eg, via dark annealing,[11] reduced peak temperature or ramp rates of fast firing,[12-15] application of high-intensity illumination at elevated temperature,[16] or phosphorus diffusion gettering of LeTID-causing impurities.[17,18]

In this work, we apply a b-Si nanostructure produced by deep reactive ion etching (DRIE) to PERC cells fabricated on typical LeTID-sensitive mc-Si material. Industrial b-Si solar cells are processed together with acidic-textured references following the standard PERC process at the production line of SolarWorld Industries GmbH. In order to evaluate the strength of LeTID in cells with different surface texture and front surface passivation, the recombination properties of the cells and the resulting electrical performance both at material and device level are characterized, both initially and when exposed to commonly-used degradation conditions.[7]

2 | EXPERIMENTAL PROCEDURES

Industrial b-Si solar cells were fabricated following the standard PERC process (outlined in Figure 1) from material, which was known to be prone to LeTID. More than 100 industrial-size (156 × 156 mm) 180-µm-thick mc-Si wafers were taken from a single column of an ingot close to each other near the ingot center. The cells were divided into groups A and B depending on the used surface texture (acidic texture or b-Si, respectively). In Group B (B1 and B2), saw damage was first removed from slurry-cut mc-Si wafers by etching ~10 µm from each side in potassium hydroxide (KOH), followed by hydrochloric acid (HCl) and hydrofluoric acid-ozone (HF/O_3) cleanings. A b-Si nanostructure was etched on the front sides by DRIE using a process based on that reported in Repo et al.[4] The resulting surface morphology is presented in a scanning electron microscope (SEM) image in Figure 1. Due to clamping against the bottom electrode, approximately 5 mm from each wafer edge remained unetched. Additionally, the adaption of the b-Si fabrication process to a larger substrate area resulted in an increased silicon consumption, and ~15 µm was removed from the wafer front surface. In Group A (A1 and A2), instead of saw damage removal (SDR) and b-Si etching, the wafers were textured acidically in hydrofluoric-nitric acid (HF/HNO_3) solution, which etched ~5 µm from both sides of the wafer. After cleaning, all Group A and B wafers were merged into a single batch, and phosphorus emitter was formed by $POCl_3$ diffusion. The large surface area of b-Si resulted in a heavier emitter in the b-Si wafers (~50 Ω/□ vs ~80 Ω/□, as determined by four-point probe), which agrees with earlier reports.[19-21] Although the wafers were diffused back-to-back, emitter formation was followed by etching of ~5 µm from the rear side with HF/HNO_3 solution to ensure the absence of a phosphorus-doped layer at the rear and to enhance internal reflection. Phosphosilicate glass was removed in HF, which was followed by cleaning with diluted HF. The cleaning was kept dilute intentionally, since standard cleaning solutions etch heavily phosphorus-doped b-Si at a rapid rate, and hence, alter the electrical and optical properties of the front surface.[22] The back side was passivated with an AlO_x/SiN_x stack.

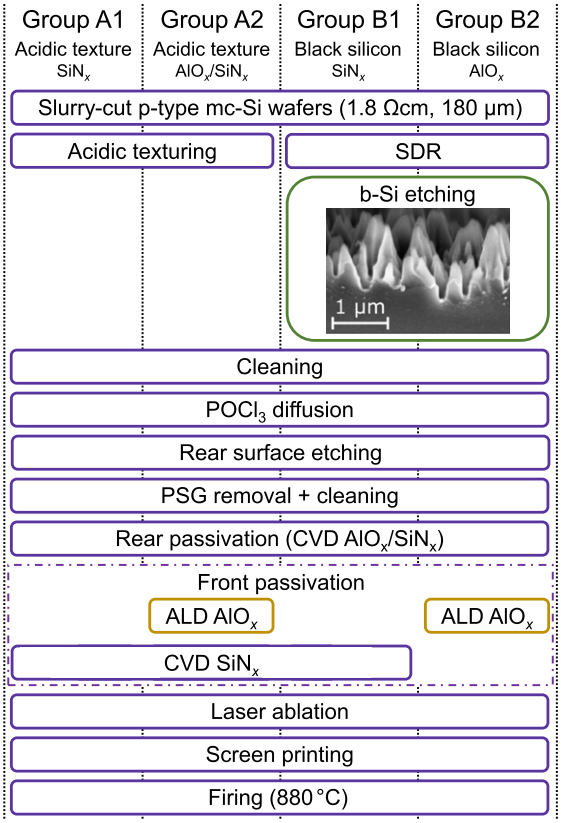

FIGURE 1 Process flow chart. PERC cells were fabricated mainly at an industrial production line (purple outline). Black silicon was etched using a lab-scale single-wafer equipment, and ALD coating was deposited with a large-scale batch tool. The b-Si morphology is presented in a SEM image [Colour figure can be viewed at wileyonlinelibrary.com]

Front surfaces of group A2 and B2 cells were passivated with 30 nm of ALD AlO_x deposited at 275°C, whereas group A1 and B1 cells were coated with a standard industrial plasma-enhanced (remote plasma) chemical vapor deposited (PECVD) SiN_x anti-reflection film. Group A2 cells were additionally capped with a PECVD SiN_x coating to reduce reflectance, while the corresponding b-Si cells (group B2) were left without additional thin films. After front surface passivation and rear contact opening, all wafers were screen printed and fired at 880°C (set point temperature). Screen dimensions were slightly reduced from the standard size according to the dimensions of the b-Si area to have metallization only on b-Si. The cells were mainly processed at the industrial production line of SolarWorld Industries GmbH with two exceptions (highlighted with different color in Figure 1): b-Si was etched with a lab-scale (~15 min/wafer) single-wafer equipment (Oxford Instruments Plasmalab System 100) at Aalto University, and ALD AlO_x was deposited using a large-scale batch tool (Beneq P400) at Beneq Oy.

The complete cells were characterized under the standard test conditions (25°C, 1000 W/m^2, AM1.5 spectrum) by current-voltage (I-V) measurements, from which typical solar cell parameters were determined, including power conversion efficiency (η), open-circuit

voltage (V_{oc}) and short-circuit current density (J_{sc}). The cells were degraded under 0.5 sun illumination at 75°C for 1 week (~160 hours), during which the I-V characteristics were measured at regular intervals. In addition, internal quantum efficiency spectra (IQE) and photoluminescence (PL) maps were measured from each cell, both before and after the degradation.

3 | RESULTS AND DISCUSSION

3.1 | Quantum efficiency and bulk properties

Figure 2A presents IQE spectra of the acidic-textured cells with either SiN_x or AlO_x/SiN_x front surface passivation in the initial and degraded form. LeTID is clearly visible in both cells as a reduction in IQE under illumination at 75°C. No clear difference is observed in the degradation behavior of cells with different front surface passivation layers. The reduction in IQE is the strongest in the ~850 to 1100-nm wavelength range, which indicates that the degradation occurs in the bulk or at the rear surface. Consistently, earlier studies have suggested that LeTID is mainly a bulk effect.[12,23,24] Interestingly, both surface passivation schemes produce nearly identical IQE spectra also in the short wavelength range (both before and after degradation), although it is generally understood that AlO_x is unfavorable for phosphorus emitter passivation due to the high density of negative fixed charges in the thin film.[19,25,26] The charge polarity was indeed confirmed to be negative, and hence, surface passivation is attributed to excellent chemical passivation provided by ALD AlO_x.[27]

The b-Si cells do not show such degradation. Figure 2B,C compares IQE of acidic-textured and b-Si cells passivated with either ALD AlO_x or CVD SiN_x, respectively, in the wavelength range with most significant LeTID present (~850-1100 nm). While IQE of the acidic-textured cells declines remarkably independent of the surface passivation layer, the b-Si cells nearly perfectly retain their initial performance. In particular, the AlO_x-passivated b-Si cells show no degradation (Figure 2B), although also they have a hydrogen-rich AlO_x/SiN_x dielectric stack on the rear. Since ALD AlO_x contains only little hydrogen compared with CVD SiN_x,[28] the excellent stability of the AlO_x-passivated b-Si cells could be at least partly explained by a lower total amount of hydrogen diffusing into the bulk to activate the LeTID-responsible defects.[29,30] Nevertheless, b-Si cells with SiN_x front surface passivation also show only slight degradation compared with the acidic-textured equivalents (Figure 2C), and hence, the superiority of the b-Si cells over the acidic-textured equivalents after degradation cannot be attributed to different surface passivation films alone.

The complete IQE spectra of the b-Si cells, which are shown as insets in Figure 2B,C, reveal that the b-Si cells suffer from weak blue response, which can be mainly attributed to excessively heavy emitter doping. In addition to the large number of electrically active dopants in the b-Si emitters, as indicated by the sheet resistance (~50 Ω/□ vs ~80 Ω/□ for b-Si and acidic-textured cells, respectively), the b-Si spikes likely contain a significant amount of inactive phosphorus,[19] which causes excessive SRH recombination.[31] Moreover, contrary to the acidic-textured cells, negative fixed charges in ALD AlO_x impair the blue response of the AlO_x-passivated b-Si cells, since surface

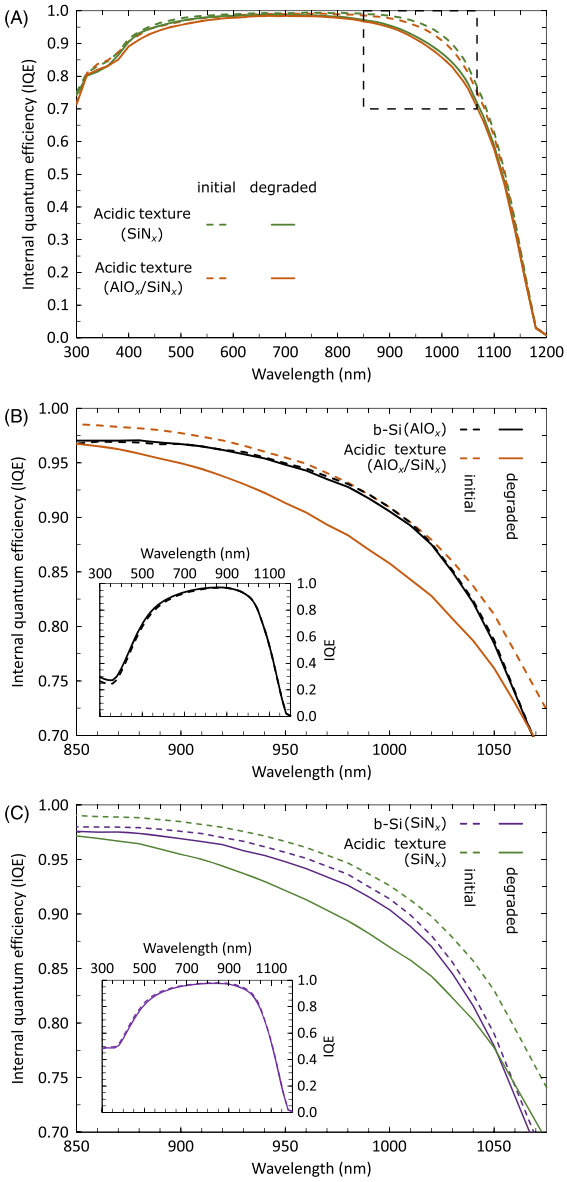

FIGURE 2 A, Internal quantum efficiency (IQE) of acidic-textured solar cells with front surface passivated with either CVD SiN_x or ALD AlO_x. B-C, Inset of the wavelength range with the largest IQE degradation (highlighted in (A)) for acidic-textured and b-Si solar cells with either (B) ALD AlO_x or (C) CVD SiN_x front surface passivation. The complete IQE spectra of the b-Si cells are presented as insets in (B) and (C). Note that the AlO_x-passivated acidic-textured cells have a SiN_x capping. All spectra are given both directly after firing (dashed lines) and after degradation (solid lines) [Colour figure can be viewed at wileyonlinelibrary.com]

passivation of b-Si relies more heavily on field-effect.[32] Nevertheless, the IQE of the AlO_x-passivated b-Si cells slightly improves during the degradation treatment especially in the short wavelength range, which is most likely due to enhanced field-effect passivation induced by increased charge density in the AlO_x thin film.[28]

The observations from IQE spectra are supported by spatially resolved PL maps. Figure 3A shows a photograph of a final b-Si PERC solar cell, and Figure 3B,C presents corresponding relative PL maps for b-Si cells passivated with either ALD AlO_x or CVD SiN_x, respectively. Correspondingly, Figure 3D,E,F shows the photograph and relative PL maps for the acidic-textured cells, with the exception that the cell

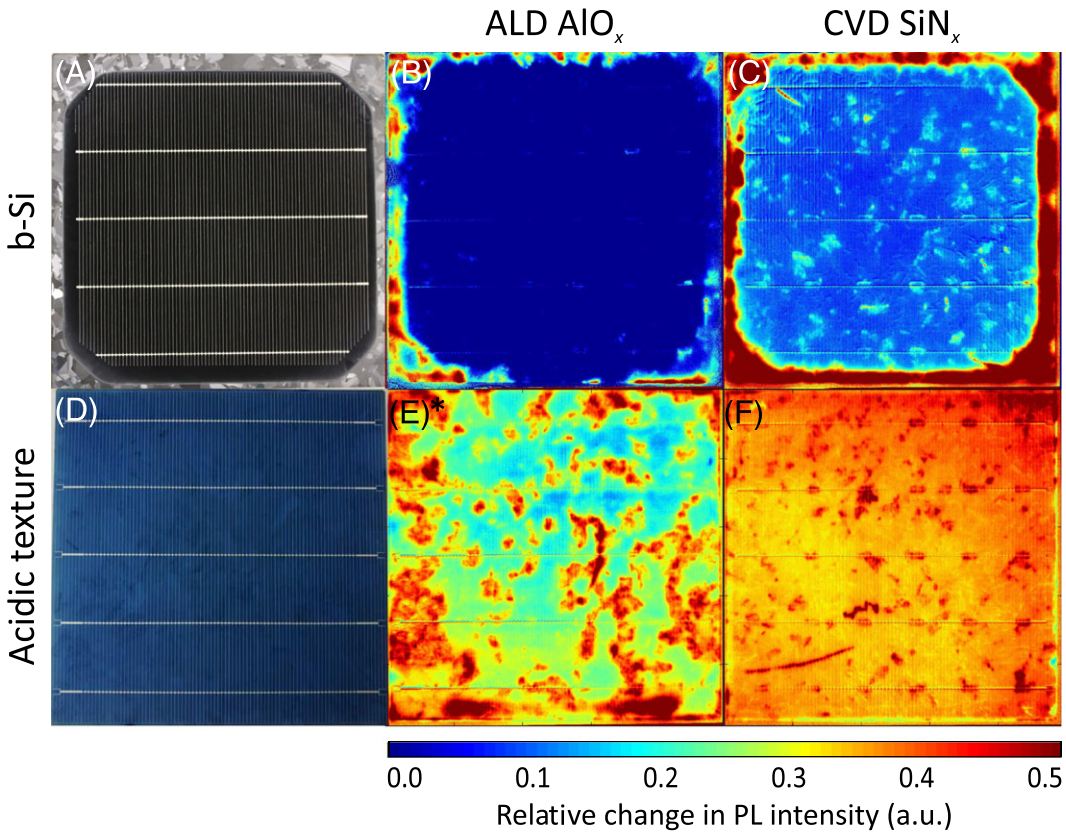

FIGURE 3 A, Photograph of a 156 × 156 mm multicrystalline b-Si PERC solar cell with AlO_x surface passivation. Approximately, 5 mm from wafer edges remained without b-Si due to clamping during the b-Si etching process. B-C, PL intensity change during degradation normalized to the initial intensity of an (B) ALD AlO_x or (C) CVD SiN_x-passivated b-Si cell. D, Photograph of a standard acidic-textured PERC with SiN_x anti-reflection coating processed in the same batch. E-F, Normalized PL intensity change during degradation of an (E) ALD AlO_x/CVD SiN_x or (F) CVD SiN_x-passivated acidic-textured cell. The same color scale applies to all maps: Red color represents a large decrease in the PL intensity indicating strong degradation, while blue color represents stable PL intensity and no degradation. *Note that the acidic-textured cell in PL map (E) has an additional SiN_x coating compared with the b-Si cell in map (B) [Colour figure can be viewed at wileyonlinelibrary.com]

with ALD AlO_x front surface passivation has a CVD SiN_x coating. The maps represent the PL intensity decrease after a 1-week degradation normalized to the initial PL intensity, ie, blue color represents no change in PL intensity, indicating no degradation in the wafer bulk, whereas red color represent the highest decrease in the PL intensity during degradation. Consistent with the IQE spectra in Figure 2B, the AlO_x-passivated b-Si cell completely retains its performance under illumination at elevated temperature (Figure 3B). Simultaneously, the edges, which were not subjected to b-Si etching, show a slight degradation. Hence, hydrogen in-diffusion from the SiN_x film on the rear is enough to activate some amount of LeTID-causing defects in the bulk on areas without b-Si. However, the degradation is more severe with SiN_x front passivation (Figure 3C), as expected.[29,30,33] Nevertheless, the b-Si area degrades only slightly, while the non-textured edges show significant deterioration. This agrees with the IQE spectra (Figure 2C) and confirms that the reduced degradation in the b-Si cells cannot be explained only by a different amount of hydrogen in the surface passivation layers.

The PL images show also that both acidic-textured cells degrade more than either of the b-Si cells (Figure 3E,F). However, contrary to the IQE spectra in Figure 2A, the acidic-textured cell with CVD SiN_x front surface passivation (Figure 3F) shows on average more severe degradation than the equivalent with an ALD AlO_x interlayer (Figure 3E). This observation suggests that 30 nm of ALD AlO_x is thick and dense enough to impede hydrogen diffusion from SiN_x to the silicon bulk,[34] contrary to earlier reports for CVD AlO_x[33] or thinner ALD films.[29] Hence, hydrogen can mainly diffuse in the wafer only from the rear side through the CVD AlO_x film, resulting in weaker LeTID. Alternatively, the charge polarity in the thin film may have an effect, since both plasma-enhanced CVD SiN_x and ALD AlO_x are known to getter metal impurities.[35,36] Nevertheless, the largest degradation is observed in the non-textured edges of the SiN_x-passivated b-Si cells, which is an interesting finding and will be discussed later in more detail. Finally, Figure 3C reveals that the degradation is rather uniform laterally in good grain areas, which is characteristic of LeTID.[12,14] However, defect clusters show slightly stronger LeTID, as reported recently,[37,38] which is even more pronounced in the acidic-textured cells (Figure 3E,F).

3.2 | Current-voltage characteristics

The lower magnitude of LeTID in b-Si cells is also reflected in cell efficiency and other essential solar cell parameters, such as V_{oc} and I_{sc}. Figure 4 compares the evolution of power conversion efficiency of b-Si and acidic-textured cells normalized to the initial efficiency

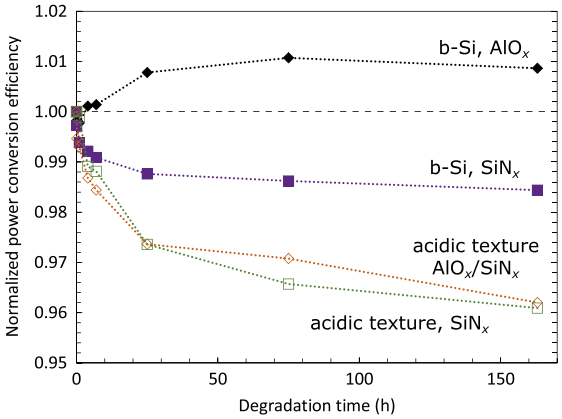

FIGURE 4 Power conversion efficiency of ALD AlO_x or CVD SiN_x-passivated b-Si and acidic-textured cells as a function of degradation time normalized to the initial efficiency. The dotted lines act as a guide for the eye [Colour figure can be viewed at wileyonlinelibrary.com]

measured throughout a 1-week degradation. As expected from the IQE spectra (Figure 2A) and PL maps (Figure 3E,F), the efficiencies of both acidic-textured cells decline significantly (nearly $4\%_{rel}$) under 0.5 sun illumination at 75°C. Additionally, the AlO_x interlayer has only modest effect on the degradation trend, and the AlO_x/SiN_x-passivated cell slightly outperforms the SiN_x-passivated equivalent, which is in agreement with the PL maps. The magnitude and time scale of the degradation agree with earlier reports on LeTID.[7,10] The cells show no regeneration until the end of the 1-week degradation cycle, which is natural, since complete saturation is not yet reached. On the other hand, the AlO_x-passivated b-Si cells not only retain their performance, but their efficiency even improves by ~$1\%_{rel}$, which is most likely due to enhanced field-effect passivation as concluded earlier from the IQE behavior. Likewise, the SiN_x-passivated b-Si cells are substantially more stable than either of the acidic-textured cells with only $1.5\%_{rel}$ degradation, consistent with both IQE spectra and PL maps. Similar trends are visible also in V_{oc} and I_{sc} of the cells.

Finally, Table 1 presents the cell parameters of the AlO_x or SiN_x-passivated b-Si and acidic-textured cells measured directly after firing and their absolute change during a 1-week degradation. The best performance is obtained with b-Si texture and SiN_x passivation, despite a slight degradation. Furthermore, both b-Si cells maintain their level of performance substantially better than either of the acidic-textured cells in all relevant solar cell parameters. However, the AlO_x-passivated cells suffer from increased contact resistance due to challenges in screen-printing through a 30-nm-thick ALD AlO_x layer, which is expected, as even 10-nm films have been reported to increase contact resistance losses independent of firing temperature.[39] This is seen as reduced fill factor, which is pronounced in the acidic-textured cells due to the additional SiN_x film. Moreover, the excessively heavy emitter doping likely reduces the V_{oc} of the b-Si cells, which was observed also in IQE (Figure 2B,C). The effect is even more pronounced in the AlO_x-passivated b-Si cells due to the non-optimal charge polarity for phosphorus emitter passivation. Interestingly, both SiN_x-passivated cells reach approximately the same V_{oc} after degradation. Nevertheless, while also bulk quality affects V_{oc}, the low V_{oc} of the b-Si cells can be mainly attributed to poor electrical performance at the front surface, since the long-wavelength IQE (Figure 2B-C) and PL maps (Figure 3B-C and 3E-F) indicate higher bulk quality in the b-Si cells after degradation.

The efficiency of the AlO_x/SiN_x-passivated acidic-textured cells is further lowered by optically unfavorable total thickness of the AlO_x/SiN_x dielectric stack, which heavily reduces J_{sc}. Since fair comparison between different cell types was prioritized instead of specifically optimized b-Si cell process, none of the process steps were particularly adjusted for b-Si surfaces. Hence, the performance of the b-Si cells could be further improved by optimization of, eg, emitter diffusion and front side metallization.

3.3 | Physical background for impact of b-Si on LeTID

The results demonstrate that the amount of LeTID is reduced by the application of b-Si, indicating that the defect responsible for the phenomenon must be in an inactive state or removed in the b-Si cells. Next, we discuss possible explanations for the capability of b-Si to reduce LeTID.

Recent studies suggest that P or Al-gettering can suppress LeTID to some extent,[17,18] especially in material with low lifetime.[37] Zuschlag et al showed that P-diffused SiN_x-passivated mc-Si lifetime samples experienced only slight degradation, whereas a stronger and faster LeTID was observed in ungettered sister samples.[17] Chakraborty et al presented similar results and reported that phosphorus diffusion gettering reduced the concentration of light-induced defects, which were suspected to be Cu, Ni, and Ti, by nearly one order of magnitude.[18] Interestingly, our previous study demonstrated that heavy phosphorus-doping in the b-Si spikes after an industry-typical $POCl_3$ diffusion process enhances iron segregation to the emitter, which substantially improves minority carrier lifetime in iron-contaminated substrates.[6] Consistent with earlier reports,[19-21] sheet resistance is indeed substantially lower in the b-Si than in the acidic-textured cells (~50 Ω/□ vs ~80 Ω/□). Thus, the reduced LeTID could be at least partly explained by a heavier phosphorus emitter, and hence enhanced gettering, in the b-Si cells,[6] although the defect responsible for the

TABLE 1 Cell parameters of b-Si and acidic-textured solar cells with different front surface passivation directly after firing (initial) and amount of degradation in absolute values. The reduced active area of the b-Si cells is taken into account in the reported efficiency

		η		V_{oc}		J_{sc}		FF	
		Initial (%)	Change ($\%_{abs}$)	Initial (mV)	Change (mV)	Initial (mA/cm^2)	Change (mA/cm^2)	Initial	Change
Black silicon	AlO_x	17.2	+0.2	613	+1.4	36.5	+0.2	76.9	+0.1
	SiN_x	18.8	−0.3	635	−3.0	37.7	−0.4	78.6	−0.1
Acidic texture	AlO_x/SiN_x	14.5	−0.6	636	−8.8	35.0	−0.6	65.2	−0.5
	SiN_x	18.7	−0.7	643	−10.7	36.6	−0.6	79.3	−0.6

degradation is likely another impurity than Fe.[40,41] This explanation supports the conclusion that LeTID is a bulk effect, as suggested previously,[12,23,24] instead of, eg, deterioration of rear surface passivation.

Additionally, gettering may be intensified also by accumulation of impurities at the AlO_x–Si interface or into the SiN_x bulk during post-deposition heat treatments.[35,36] This may have a stronger effect in b-Si, since the large surface area of the nanostructure provides more gettering sites at the dielectric-Si interface. Furthermore, the negative fixed charges in ALD AlO_x are known to generate an enhanced electric field in b-Si due to conformal coating on the high aspect ratio nanostructures,[32] which may affect impurity gettering.

In addition to beneficial gettering of defects within the silicon wafer, application of b-Si may remove the deleterious impurities altogether. In typical acidic texturing, saw damage resulting from slurry-based wire sawing is used as an initiator for the texture etching process.[42] However, saw damage may contain detrimental contaminants, such as copper,[43,44] which lead to the following degradation.[45] Instead, fabrication of b-Si by DRIE is independent of the initial surface condition,[46,47] which allows a complete removal of the contaminated surface layers. In this work, saw damage was removed from the b-Si cell precursors as a separate wet-chemical etching step prior to texturization in order to remove the damage also from the wafer edges, which were not etched during b-Si fabrication. Nevertheless, since a clear contrast between the b-Si area and the unetched edges is visible in the PL maps, especially in that of the SiN_x-passivated b-Si cell (Figure 3C), the separate SDR alone cannot explain the difference between cells with different textures, but the reduced LeTID is likely a b-Si related phenomenon.

Due to the increased silicon consumption of the applied b-Si fabrication process, the final b-Si cell thickness was decreased to ~140 μm, which appears as a dip in IQE at long wavelengths (Figure 2B,C). The acidic-textured cells are slightly thicker, ~165 μm, while the non-textured edges of the b-Si cells, which experienced SDR instead of acidic-texturing, have a final thickness between these two (~155 μm). Interestingly, Bredemeier et al reported that wafer thinning reduces LeTID-causing effective defect density.[41] In our experiments, the non-textured edges of the SiN_x-passivated b-Si cells show more pronounced degradation in the PL map (Figure 3C) than the thicker acidic-textured cells (Figure 3F). Hence, the magnitude of LeTID in our cells seems to scale rather with surface area than wafer thickness: b-Si cells with the largest surface area (ratio to polished surface $S_f \approx 5–7$[32,48]) experience the weakest degradation, followed by acidic-textured cells ($S_f \approx 2$[49,50]), and the strongest LeTID is shown at the edges of b-Si cells, which were chemically polished by SDR. Nevertheless, we want to stress that the heavy silicon consumption is a feature of the specific b-Si etching process used in this study and could be drastically reduced by further optimization of the DRIE process. The reduced IQE in the b-Si cells may be also contributed by weaker light-trapping due to the nanometer-scale dimensions of the nanostructure, which could be enhanced by coupling b-Si with micrometer-sized pyramid texture.[51]

Another important aspect affecting the magnitude of LeTID is the applied firing process.[12-15] Although the cells are fired with identical set peak temperature and profile, the actual temperature reached by the wafers may vary due to differences in optics of the front surface or wafer thickness. Indeed, the higher absorbance of b-Si compared with either of the AR-coated acidic-textured surfaces indicates that b-Si cells may reach a higher temperature during firing. Correspondingly, a thinner wafer may heat up more compared with a thicker one due to the smaller volume of the wafer, although recent results[41] report thinner samples to experience weaker LeTID. Hence, the possible effect of surface texture or wafer thickness on the actual firing temperature experienced by the wafers should be visible only as more intense LeTID in the b-Si cells. Thus, the difference between the b-Si and acidic-textured cells could be even larger if the actual wafer temperatures were exactly identical. Furthermore, since the set peak firing temperature was 880°C, it is highly unlikely that any of the cells would have experienced a temperature lower than the threshold for LeTID (720°C-740°C[52,53]).

4 | CONCLUSIONS

This work demonstrated that a b-Si nanostructure reduces the amount of LeTID in industrial p-type mc-Si PERC. Acidic-textured reference cells showed clear degradation in IQE independent of charge polarity in the front surface passivation film (SiN_x or AlO_x/SiN_x), especially in the ~850 to 1100-nm wavelength range, which suggests that the degradation occurred in the bulk. Instead, the b-Si cells retained their performance nearly perfectly, despite the presence of a hydrogen-rich AlO_x/SiN_x passivation stack on the rear. Especially, the b-Si cells with ALD AlO_x front surface passivation showed no degradation, which may be in part due to a lower total amount of in-diffused hydrogen in the bulk, preventing the activation of LeTID-responsible defects.[28,29] Furthermore, the presence of a hydrogen-rich SiN_x film on the front induced only slight degradation in the b-Si cells compared with the acidic-textured equivalents. The observations were supported by spatially resolved PL imaging, which showed a clear contrast between the b-Si and acidic-textured cells after degradation, especially in the case of SiN_x front surface passivation.

The lower magnitude of LeTID eventually reflected to the power conversion efficiency of the b-Si solar cells. The efficiency of the AlO_x-passivated b-Si PERC increased by $1\%_{rel}$ under a 1-week illumination at 75°C, most likely due to enhanced front surface passivation. Simultaneously, the SiN_x-passivated b-Si cells lost only $1.5\%_{rel}$ of their initial efficiency, while the acidic-textured equivalents degraded by nearly $4\%_{rel}$. Although the exact mechanism for LeTID mitigation by b-Si remained unresolved, the phenomenon could be contributed by the strong ability of b-Si to getter LeTID-causing impurities. Indeed, the PL maps suggested that the magnitude of LeTID scales with surface area. Furthermore, hydrogen-rich SiN_x anti-reflection coatings can be replaced by ALD AlO_x due to the negligible reflectance of b-Si, which aids to suppress LeTID efficiently. Since the majority of the cell processing was performed at an industrial production line, the results should be of direct interest to PV industry.

ACKNOWLEDGEMENTS

The authors acknowledge the provision of facilities by Aalto University at OtaNano—Micronova Nanofabrication Centre. This work was partially funded by project "BLACK" (project no. 2956/31/2014),

which was supported under the umbrella of SOLAR-ERA.NET by Business Finland (former Tekes—the Finnish Funding Agency for Innovation), and partially through the European Research Council under the European Union's FP7 Programme ERC grant agreement no. 307315. T. P. Pasanen acknowledges the Aalto ELEC Doctoral School, Jenny and Antti Wihuri Foundation, and Walter Ahlström Foundation for the financial support. H. S. Laine acknowledges the support of the Finnish Cultural Foundation, Tiina & Antti Herlin Foundation, and Walter Ahlström Foundation.

ORCID

Toni P. Pasanen http://orcid.org/0000-0003-1218-7303
Ville Vähänissi http://orcid.org/0000-0002-2681-5609
Ismo T.S. Heikkinen http://orcid.org/0000-0002-3414-9394

REFERENCES

1. Liu X, Coxon PR, Peters M, Hoex B, Cole JM, Fray DJ. Black silicon: fabrication methods. *Properties Solar Energy Appl Energy Environ Sci*. 2014;7:3223-3263.
2. International technology roadmap for photovoltaic. *Results 2016*. 8th ed. ; 2017.
3. Otto M, Kroll M, Käsebier T, Salzer R, Tünnermann A, Wehrspohn RB. Extremely low surface recombination velocities in black silicon passivated by atomic layer deposition. *Appl Phys Lett*. 2012;100(19):191603.
4. Repo P, Haarahiltunen A, Sainiemi L, et al. Effective passivation of black silicon surfaces by atomic layer deposition. *IEEE J Photovolt*. 2013;3(1):90-94.
5. Savin H, Repo P, von Gastrow G, et al. Black silicon solar cells with interdigitated back-contacts achieve 22.1% efficiency. *Nat Nanotechnol*. 2015;10(7):624-628.
6. Pasanen TP, Laine HS, Vähänissi V, Schön J, Savin H. Black silicon significantly enhances phosphorus diffusion gettering. *Sci Rep*. 2018;9:1991. https://doi.org/10.1038/s41598-018-20494-y
7. Kersten F, Engelhart P, Ploigt HC, et al. Degradation of multicrystalline silicon solar cells and modules after illumination at elevated temperature. *Sol Energy Mater Sol Cells*. 2015;142:83-86.
8. Lindroos J, Savin H. Review of light-induced degradation in crystalline silicon solar cells. *Sol Energy Mater Sol Cells*. 2016;147:115-126.
9. Ramspeck K, Zimmermann S, Nagel H, Metz A, Gassenbauer Y, Birkmann B, Seidl A. Light induced degradation of rear passivated mc-Si solar cells. in Proceedings of the 27th European Photovoltaic Solar Conference and Exhibition, Frankfurt, Germany, 2012, pp. 861–865.
10. Fertig F, Krauß K, Rein S. Light-induced degradation of PECVD aluminium oxide passivated silicon solar cells. *Phys Status Solidi RRL*. 2015;9(1):41-46.
11. Chan C, Fung TH, Abbott M, et al. Modulation of carrier-induced defect kinetics in multi-crystalline silicon PERC cells through dark annealing. *Sol RRL*. 2017;1:1600028(2).
12. Nakayashiki K, Hofstetter J, Morishige AE, et al. Engineering solutions and root-cause analysis for light-induced degradation in p-type multicrystalline silicon PERC modules. *IEEE J Photovolt*. 2016;6(4):860-868.
13. Eberle R, Kwapil W, Schindler F, Schubert MC, Glunz SW. Impact of the firing temperature profile on light induced degradation of multicrystalline silicon. *Phys Status Solidi RRL*. 2016;10(12):861-865.
14. Bredemeier D, Walter D, Herlufsen S, Schmidt J. Lifetime degradation and regeneration in multicrystalline silicon under illumination at elevated temperature. *AIP Adv*. 2016;6(3):035119.
15. Vargas C, Kim K, Coletti G, et al. Carrier-induced degradation in multicrystalline silicon: dependence on the silicon nitride passivation layer and hydrogen released during firing. *IEEE J Photovolt*. 2018;8(2):413-420.
16. Payne DNR, Chan CE, Hallam BJ, et al. Rapid passivation of carrier-induced defects in p-type multi-crystalline silicon. *Sol Energy Mater Sol Cells*. 2016;158:102-106.
17. Zuschlag A, Skorka D, Hahn G. Degradation and regeneration in mc-Si after different gettering steps. *Prog Photovolt Res Appl*. 2017;25(7):545-552.
18. Chakraborty S, Huang Y, Wilson M, Aberle AG, Li JB. Mitigating light and elevated temperature induced degradation in multicrystalline silicon wafers and PERC solar cells using phosphorus diffusion gettering. *Phys Status Solidi a*. 2018;215(13):1800160.
19. Pasanen T, Vähänissi V, Theut N, Savin H. Surface passivation of black silicon phosphorus emitters with atomic layer deposited SiO_2/Al_2O_3 stacks. *Energy Procedia*. 2017;124:307-312.
20. Oh J, Yuan H-C, Branz HM. An 18.2%-efficient black-silicon solar cell achieved through control of carrier recombination in nanostructures. *Nat Nanotechnol*. 2012;7(11):743-748.
21. Kafle B, Schön J, Fleischmann C, et al. On the emitter formation in nanotextured silicon solar cells to achieve improved electrical performances. *Sol Energy Mater Sol Cells*. 2016;152:94-102.
22. Pasanen TP, Laine HS, Vähänissi V, Salo K, Husein S, Savin H. Impact of standard cleaning on electrical and optical properties of phosphorus-doped black silicon. *IEEE J Photovolt*. 2018;8:697-702.
23. Padmanabhan M, Jhaveri K, Sharma R, et al. Light-induced degradation and regeneration of multicrystalline silicon Al-BSF and PERC solar cells. *Phys Status Solidi RRL*. 2016;10(12):874-881.
24. Luka T, Turek M, Großer S, Hagendorf C. Microstructural identification of cu in solar cells sensitive to light-induced degradation. *Phys Status Solidi RRL*. 2017;11. 16000426. https://doi.org/10.1002/pssr.201600426
25. Hoex B, Gielis JJH, van de Sanden MCM, Kessels WMM. On the c -Si surface passivation mechanism by the negative-charge-dielectric Al_2O_3. *J Appl Phys*. 2008;104(11):113703.
26. van de Loo BWH, Knoops HCM, Dingemans G, et al. "Zero-charge" SiO_2/Al_2O_3 stack for the simultaneous passivation of n^+ and p^+ doped silicon surfaces by atomic layer deposition. *Sol Energy Mater Sol Cells*. 2015;143:450-456.
27. Hoex B, van de Sanden MCM, Schmidt J, Brendel R, Kessels WMM. Surface passivation of phosphorus-diffused n^+-type emitters by plasma-assisted atomic-layer deposited Al_2O_3. *Phys Status Solidi RRL*. 2012;6(1):4-6.
28. Dingemans G, Engelhart P, Seguin R, et al. Stability of Al_2O_3 and Al_2O_3/a-SiN_x:H stacks for surface passivation of crystalline silicon. *J Appl Phys*. 2009;106(11):114907.
29. Bredemeier D, Walter DC, Schmidt J. Lifetime degradation in multicrystalline silicon under illumination at elevated temperature: indications for the involvement of hydrogen. AIP Conf Proc 2018;1999:130001.
30. Winter C, Zuschlag A, Skorka D, Hahn G. Influence of dielectric layers and thermal load on LeTID. AIP Conf Proc. 2018;1999:130020.
31. Min B, Wagner H, Dastgheib-Shirazi A, Altermatt PP. Limitation of industrial phosphorus-diffused emitters by SRH recombination. *Energy Procedia*. 2014;55:115-120.
32. von Gastrow G, Alcubilla R, Ortega P, et al. Analysis of the atomic layer deposited Al_2O_3 field-effect passivation in black silicon. *Sol Energy Mater Sol Cells*. 2015;142:29-33.
33. Kersten F, Heitmann J, Müller JW. Influence of Al_2O_3 and SiN_x passivation layers on LeTID. *Energy Procedia*. 2016;92:828-832.
34. Wilking S, Herguth, A, Hahn G. Influence of hydrogen on the regeneration of boron-oxygen related defects in crystalline silicon. *J Appl Phys*. 2013;113(19):194503.
35. Liu AY, Sun C, Markevich VP, Peaker AR, Murphy JD, Macdonald D. Gettering of interstitial iron in silicon by plasma-enhanced chemical vapour deposited silicon nitride films. *J Appl Phys*. 2016;120(19):193103.

36. Liu AY, Macdonald D. Impurity gettering effect of atomic layer deposited aluminium oxide films on silicon wafers. *Appl Phys Lett*. 2017;110(19):191604.
37. Skorka D, Zuschlag A, Hahn G. Firing and gettering dependence of effective defect density in material exhibiting LeTID. AIP Conf Proc. 2018;1999:130015.
38. Lindroos J, Zuschlag A, Carstensen J, Hahn G. Light-induced degradation variation in industrial multicrystalline PERC silicon solar cells. AIP Conf Proc. 2018;1999:130013.
39. To A, Li WM, Li X, Hoex B. The effects of bifacial deposition of ALD AlO_x on the contact properties of screen-printed contacts for *p*-type PERC solar cells. *Energy Procedia*. 2017;124:914-921.
40. Morishige AE, Jensen MA, Needleman DB, et al. Lifetime spectroscopy investigation of light-induced degradation in p-type multicrystalline silicon PERC. *IEEE J Photovolt*. 2016;6(6):1466-1472.
41. Bredemeier D, Walter DC, Schmidt J. Possible candidates for impurities in mc-Si wafers responsible for light-induced lifetime degradation and regeneration. *Sol RRL*. 2017;2. 1700159. https://doi.org/10.1002/solr.201700159
42. Hauser A, Melnyk I, Fath P, Narayanan S, Roberts S, Bruton TM. A simplified process for isotropic texturing of mc-Si. Proceedings of 3rd World Conference on Photovoltaic Energy Conversion, Osaka, Japan, 2003;2:1447–1450.
43. Vahlman H, Wagner M, Wolny F, et al. Light-induced degradation in quasi-monocrystalline silicon PERC solar cells: indications on involvement of copper. *Phys Status Solidi a*. 2017;214(7):1700321.
44. Buchholz F, Wefringhaus E, Schubert G. Metal surface contamination during phosphorus diffusion. *Energy Procedia*. 2012;27:287-292.
45. Lindroos J, Bouldrad Y, Yli-Koski M, Savin H. Preventing light-induced degradation in multicrystalline silicon. *J Appl Phys*. 2014;115(15):154902. https://doi.org/10.1063/1.4871404
46. Jansen H, de Boer M, Legtenberg R, Elwenspoek M. The black silicon method: a universal method for determining the parameter setting of a fluorine-based reactive ion etcher in deep silicon trench etching with profile control. *J Micromech Microeng*. 1995;5(2):115-120.
47. Sainiemi L, Jokinen V, Shah A, et al. Non-reflecting silicon and polymer surfaces by plasma etching and replication. *Adv Mater*. 2011;23(1):122-126.
48. von Gastrow G, Ortega P, Alcubilla R, et al. Recombination processes in passivated boron-implanted black silicon emitters. *J Appl Phys*. 2017;121(18):185706.
49. Reichel C, Granek F, Benick J, Schultz-Wittmann O, Glunz SW. Comparison of emitter saturation current densities determined by injection-dependent lifetime spectroscopy in high and low injection regimes. *Prog Photovolt Res Appl*. 2012;20(1):21-30.
50. Kafle B, Freund T, Mannan A, et al. Plasma-free dry-chemical texturing process for high-efficiency multicrystalline silicon solar cells. *Energy Procedia*. 2016;92:359-368.
51. Peyronnet R, Fischer G, Blévin T, Johnson EV, Drahi E, Lemiti M. Texturing optimization for bifacial n-PERT: are pyramids and/or black silicon the way to go for thinner devices? *Energy Procedia*. 2017;120:250-259.
52. Herguth A, Keller P, Mundhaas N. Influence of temperature on light induced phenomena in multicrystalline silicon. AIP Conf Proc. 2018;1999:130007.
53. Kim M, Chen D, Abbott M, Wenham S, Hallam B. Role of hydrogen: formation and passivation of meta-stable defects due to hydrogen in silicon. AIP Conf Proc. 2018;1999:130010.

How to cite this article: Pasanen TP, Modanese C, Vähänissi V, et al. Impact of black silicon on light- and elevated temperature-induced degradation in industrial passivated emitter and rear cells. *Prog Photovolt Res Appl*. 2019;27:918–925. https://doi. org/10.1002/pip.3088